ISSN 1746-7659, England, UK
Journal of Information and Computing Science
Vol. 17, No. 1, 2022, *pp*.064-074

Affine Invariant Representation with Generic Polar Radius Integral Transform

Chunyan Liu [1], Jianwei Yang [1,2] ,Chengxi Zhou[3]

[1]School of Mathematics and Statistics, Nanjing University of Information Science and Technology, Nanjing, China, 210044

[2]Guangdong Key Laboratory of Intelligent Information Processing and Shenzhen Key Laboratory of Media Security, Shenzhen , China, 518060

[3]Jiayuan Technology Co., Ltd, Nanjing, China, 210019

(Received February 07, 2022, accepted April 19, 2022)

Abstract: In many computer vision tasks, the extraction of features invariant to affine transform plays an important role. To achieve better accuracy, region-based approaches usually need expensive computation. Whereas, contour-based methods need less computation, but their performance is strongly dependant on the boundary extraction. A method, *generic polar radius integral transform* (GPRIT), is proposed to combine region-based and contour-based method together for the extraction of affine invariant features. Polar radius integral transform and central projection transform are all special cases of the proposed GPRIT. With GPRIT, any object is converted into a closed curve for data reduction. Consequently, stationary wavelet transform is conducted to construct affine invariants. Several experiments have been presented to evaluate performance of the proposed GPRIT.

Keywords: *generic polar radius integral transform* (GPRIT), invariant, affine transform, feature extraction.

1. Introduction

Image is an important communication tool and information medium in daily production and life. Image feature extraction is one of the key technologies in computer vision and pattern recognition. Affine transform, including rotation, translation, scaling and shearing transformations[1][2], can be used as the approximate model for images of the same object from different viewpoints. Affine invariant features have been applied to target recognition[3][4][5][6], image registration[7][8], digital watermarking[9][10] and many other fields. Hence, the study of affine invariant feature extraction has attracted wide attention[11][12].

To extract affine invariant features, a great number of methods have been developed. Based on whether invariant features are extracted from the contour only or from the whole shape region, these methods can be divided into categories:[13][14][15][16] contour-based and region-based. Both of these two types of methods have their merits and shortcomes.

Contour-based techniques employ boundary of objects for the extraction of invariant features, and they are often of better data reduction. Fourier descriptor[17][18] and wavelet transform[19][20][21] are two widely utilized contour-based technique. But contour-based methods are strongly dependant on the extraction of contours. They are usually invalid to objects which are consisting of several components. Consequently, applications of contour-based methods are limited.

In contrast to contour-based techniques, region-based approaches usually get high accuracy, but some of these approaches are of high computational demands. *Affine moment invariants* (AMIs)[22][23] are the most famous region-based method. But AMIs are sensitive to noise. To improve robustness of moment-based techniques to noise, *cross-weighted moment* (CWM)[24] and *multi-scale autoconvolution* (MSA)[25] have been put forward. But the computational cost of these methods are extremely expensive.

In this paper, *generic polar radius integral transform* (GPRIT) is proposed to combine contour-based technique with region-based technique. By GPRIT, any object is converted into a closed curve. All pixels in the image have been utilized. Then, parameterization and stationary wavelet transform are conducted on the obtained closed curve. The utilized technique is contour-based.

Recently, *central projection transform* (CPT)[26] and *polar radius integral transform* (PRIT)[27] have been proposed to combine region-based and contour-based techniques together. They are only special cases of the proposed GPRIT. Experiments have also been conducted to demonstrate performance of the proposed GPRIT. Results show that the derived features are invariant to affine transform. Furthermore, GPRIT with small s is more robust to noise.

The rest of this paper is organized as follows: In section 2, the definition of GPRIT is provided. The affine invariance is also discussed. Algorithm is developed for the extracting of affine invariant features in section 3. Experimental results are presented in section 4. Finally, some conclusion remarks are given in section 5.

2. GPRIT and its affine invariance

The definition of GPRIT is provided. Affine invariance of GPRIT is also discussed.

2.1. Definition of GPRIT

To conduct GPRIT on an image $I(x,y)$, the Cartesian coordinate system needs to be transformed to polar coordinate system. The origin is firstly translated to $O(x_0,y_0)$, the centroid of image $I(x,y)$. Here,

$$x_0=\frac{\iint xI(x,y)dxdy}{\iint I(x,y)dxdy},\qquad y_0=\frac{\iint yI(x,y)dxdy}{\iint I(x,y)dxdy}.$$

In polar coordinate system, $f(r,\theta)$ is utilized to denote image $I(x,y)$.

Definition 1. *For* $s\geq 0$ *and* $h,t\in R$, *the generic polar radius integral transform (GPRIT) of image* $f(r,\theta)$ *is defined as follows:*

$$g_{s,h}^{t}(\theta)=\frac{(\int r^{s}f(r,\theta)dr)^{h}}{(\int f(r,\theta)dr)^{t}}. \tag{1}$$

By Eq .(1), it can be observed that $g_{s,h}^{t}(\theta)$ is a single-valued function. The set $\{g_{s,h}^{t}(\theta)\cos\theta, g_{s,h}^{t}(\theta)\sin\theta)\,|\,\theta\in[0,2\pi)\}$ forms a closed curve in Cartesian coordinate system. As a result, GPRIT converts any object into a closed curve $g_{s,h}^{t}(\theta)$. For example, Fig. 1(a) is an image of Coil-20 and Fig. 1(b) is the GPRIT of Fig. 1(a). It is a closed curve. In this paper, GPRIT is employed to extract affine invariant features.

Remark 1. *GPRIT is the generalization of PRIT and CPT.*

In fact, if we set $s=t=0$ and $h=1$, then $g_{s,h}^{t}(\theta)$ in Eq .(1) is the same as CPT defined in [26]. If we set $t=0$, then $g_{s,h}^{t}(\theta)$ in Eq .(1) is the same as PRIT defined in [27].

2.2. Affine invariance of GPRIT

Affine transform is the transformation defined as follows

$$\begin{pmatrix}\tilde{x}\\ \tilde{y}\end{pmatrix}=\begin{pmatrix}a & b\\ c & d\end{pmatrix}\begin{pmatrix}x\\ y\end{pmatrix}+\begin{pmatrix}e\\ f\end{pmatrix}=A\begin{pmatrix}x\\ y\end{pmatrix}+\begin{pmatrix}e\\ f\end{pmatrix},$$

where $A=\begin{pmatrix}a & b\\ c & d\end{pmatrix}$ is a non-singular matrix. For perspective distortions, affine transform can be utilized as the best linear approximation model [1][2]. It includes not only similarity transform (translation, rotation and scaling), but also shearing. The following theorem shows that the proposed GPRIT keeps the affine transform relation.

Theorem 1. *For* $s\geq 0$ *and* $h\in R$, *let* $t=h(s+1)-1$, $\tilde{f}(\tilde{r},\tilde{\theta})$ *denotes the affine transformed image of* $f(r,\theta)$. *Let* $\tilde{g}_{s,h}^{t}(\tilde{\theta})$ *be GPRIT of* $\tilde{f}(\tilde{r},\tilde{\theta})$, *and* $g_{s,h}^{t}(\theta)$ *be GPRIT of* $f(r,\theta)$. *Then the following relations hold*

$$\tilde{g}^t_{s,h}(\tilde{\theta})\cos\tilde{\theta} = ag^t_{s,h}(\theta)\cos\theta + bg^t_{s,h}(\theta)\sin\theta,$$
$$\tilde{g}^t_{s,h}(\tilde{\theta})\sin\tilde{\theta} = cg^t_{s,h}(\theta)\cos\theta + dg^t_{s,h}(\theta)\sin\theta.$$

As mentioned previous, $\tilde{g}^t_{s,h}(\tilde{\theta})$ and $g^t_{s,h}(\theta)$ convert images $f(r,\theta)$ and $\tilde{f}(\tilde{r},\tilde{\theta})$ into closed curves. The above theorem shows that $\tilde{g}^t_{s,h}(\tilde{\theta})$ and $g^t_{s,h}(\theta)$ keep the affine transform relation between $f(r,\theta)$ and $\tilde{f}(\tilde{r},\tilde{\theta})$. For instance, Fig. 1(a) and Fig. 1(c) present an image in coil-20 and its affine transform. Fig. 1(b) and Fig. 1(d) show GPRIT (closed curves) derived from Fig. 1(a) and Fig. 1(c) respectively. Here $s=1, h=-3$. It can be observed that GPRITs extracted form the original image $f(r,\theta)$ and affine transformed image $\tilde{f}(\tilde{r},\tilde{\theta})$ also satisfy the same affine transform relationship.

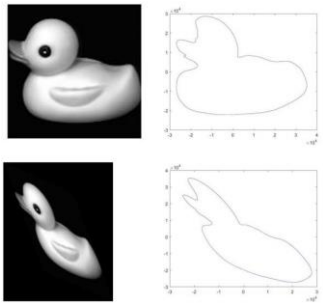

Fig. 1: (a) A gray scale image. (b) The closed curve $g^t_{s,h}(\theta)$ derived from Fig. 1(a). (c) Affine image from Fig. 1(a). (c) The closed curve $g^t_{s,h}(\theta)$ derived from Fig. 1(c).

3. The extraction of affine invariant with GPRIT

By GPRIT , a closed curve can be derived from any object. In order to apply contour-based methods to the obtained GPRIT should firstly be parameterized. Thereafter, affine invariant features could be extracted from the parameterized curve. We apply wavelet-based methods to the derived closed curve in this study.

3.1. Parameterized GPRIT

GPRIT should be parameterized to establish one-to-one points correspondence between the obtained closed curve and its affine transformed version. The curve normalization approach used in this paper mainly composes of the following steps which is called as EAN in [31]:

- For the discrete GPRIT $\{(x(\theta_k), y(\theta_k)) : k = 0,1,2,\cdots,N-1\}$, compute the total area of the closed curve by the following formula

$$S = \frac{1}{2}\sum_{k=0}^{N-1} |\, x(\theta_k)y(\theta_{k+1}) - x(\theta_{k+1})y(\theta_k)\,|.$$

  Let the number of points on the contour after EAN be N too. Denote $S_{part} = S/N$.

- Select the starting point on GPRIT as the starting point $P_0(x'(\theta_0), y'(\theta_0))$ of the normalized curve. From $P_0(x'(\theta_0), y'(\theta_0))$, search a point $P_1(x'(\theta_1), y'(\theta_1))$ along GPRIT, such that the area of each closed zone, namely the polygon P_0OP_1 equals to S_{part}, where O denotes the centroid of the object.
- Using the same method, from point $P_1(x'(\theta_1), y'(\theta_1))$, calculate all the points $P_i(x'(\theta_k), y'(\theta_k)), i \in \{1,2,\cdots,N-1\}$ along GPRIT.

3.2. Extraction of affine invariant features with wavelet transformation

We will derive affine invariant features from the normalization GPRIT by SWT.

Let $[x(\sigma), y(\sigma)]$ be the normalized GPRIT of object F_1, and $[\tilde{x}(\tilde{\sigma}), \tilde{y}(\tilde{\sigma})]$ be that of F_2, an affine transformation version of F_1. Based on the determinant properties, the basic relative invariance function can be defined as follows:

$$S(i, j, \sigma) = W_i x(\sigma) W_j y(\sigma) - W_i y(\sigma) W_j x(\sigma),$$

where W is the SWT operator, and i, j are the resolution level indexes $(i \neq j)$. The above S can be normalized as follows

$$I(i, j, \sigma) = \frac{S(i, j, \sigma)}{\|S(i, j, t)\|}, \tag{5}$$

where $\|\bullet\|$ denotes the norm of $L^2(R)$. Then $I(i, j, \sigma)$ in Eq .(5) is an absolute invariant. $I(i, j, \sigma)$ in Eq .(5) will be utilized as an invariant representation of the object. In the rest of this paper, the resolution level indexes i and j in Eq .(5) are omitted for brevity, and denote $I(i, j, \sigma)$ as $I(\sigma)$. To eliminate the effect of starting point for $I(\sigma)$, a one-dimensional Fourier-transform is applied on $I(\sigma)$. The effect of starting point is eliminated by ignoring the phase in the coefficient and only keeping the magnitudes of the coefficient.

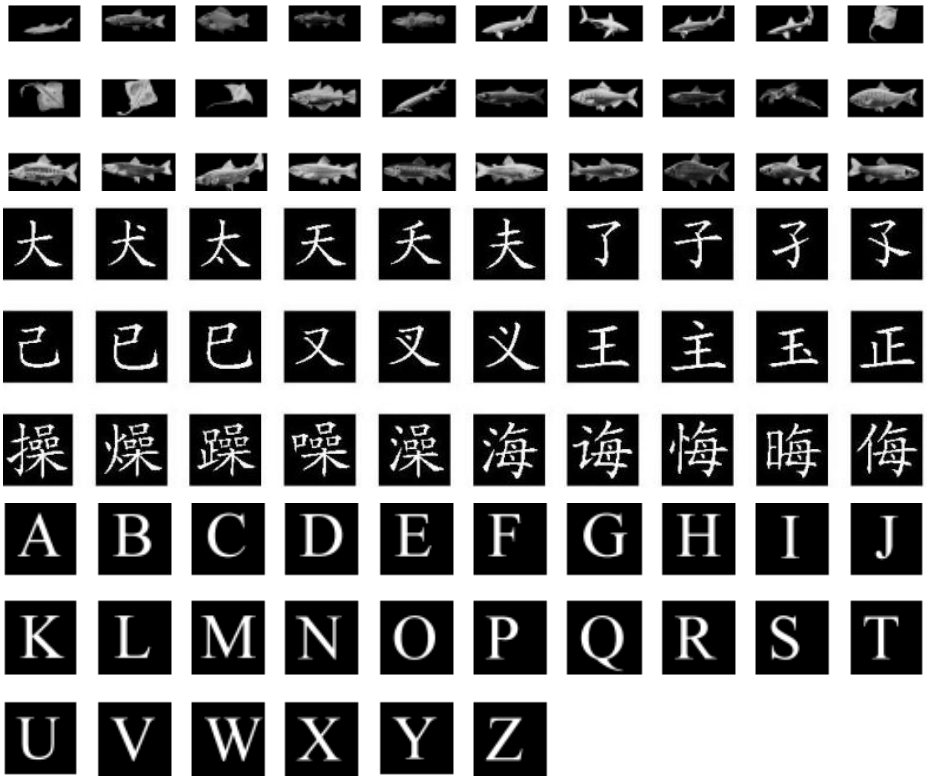

Fig. 2: (a) 30 fish images. (b) 30 Chinese characters. (c) 26 English capital letters.

4. Experiments

In this section, the proposed method is tested with the following experiments. Firstly, it is shown that the extracted features are invariant to affine transform. Secondly, we test the algorithm of affine invariant feature extraction based on GPRIT with additive noise.

Four databases of images are employed to test the performance of the proposed method. 20 images in the famous Columbia Coil-20[30] and Fig. 2(a) are employed to test performance of the proposed method to gray-scale images. Each image is size of 128×128 in Coil-20. Fig. 2(a) contains 30 fish images. The size of these images is 400×200. Fig. 2(b) and Fig. 2(c) are employed to test the performance of GPRIT to binary images. Fig. 2(b) shows 30 Chinese characters. The size of each

image in Fig. 2(b) is 256×256. Fig. 2(c) includes 26 English capital letters with Times New Roman front, and each letter is of size 256×256.

4.1. Affine invariance

In this subsection, affine invariance of the proposed method is tested with several similar Chinese characters in Fig. 2(b). Results on other images are similar.

4.2. Robustness to noise

Let $Y=(F(\theta_0),F(\theta_1),\cdots,F(\theta_{N-1}))$ be resample vector for GPRIT of image $f(r.\theta)$, and $\tilde{Y}=(\tilde{F}(\tilde{\theta}_0),\tilde{F}(\tilde{\theta}_1),\cdots,F(\tilde{\theta}_{N-1}))$ be resample vector for GPRIT of image $\tilde{f}(\tilde{r}.\tilde{\theta})$. Furthermore, set N=511. Let

$$error=\frac{\left\|Y-\hat{Y}\right\|_2}{\left\|Y\right\|_2}. \tag{6}$$

It is clearly that Eq .(6) can be used to measure the effect of noise on the general contour.

Considering the influence of the parameters of GPRIT and intensities of Gaussian noise on extraction of affine invariant features. In this experiment, we still select Coil-20[30] and Fig. 2(a) as test image. Firstly, the affine invariant features are compared with AMIs and MSA when parameter $s=1$, h is -1.00, -0.75, -0.50, -0.25, 0.00, 0.25, 0.50, 0.75, respectively. The experimental results are as shown in Table 1. Secondly, the affine invariant features are compared with AMIs when parameter $h=-1$, s is 0, 0.25, 0.50, 0.75, 1.00 ,1.25, 1.50, 1.75, 2.00, respectively. In this experiment, AMIs method takes 3 affine invariants and MSA method selects 29 affine invariants, the mean value of Gaussian noise is 0, and intensities of Gaussian noise are 0.001, 0.002, 0.003, 0.004, 0.005, and 0.006, respectively. According to Eq .(6), relative errors of GPRIT before and after adding Gaussian noise are calculated. The experimental results are as shown in Table 2. Here that no matter how s and h change, relative errors of GPRIT are smaller than that of AMIs and MSA with the increase of noise. That is to say, robustness of GPRI is better.

Considering the influence of the parameters of GPRIT and the level of 'salt&pepper' noise on extraction of affine invariant features. In this experiment, we still select 30 character images and 26 English capital letters as test images. Firstly, the affine invariant features are also compared with AMIs and MSA when parameter $s=1$, h is -1, -0.75, -0.50, -0.25, 0.00, 0.25, 0.50, 0.75, respectively. The experimental results are as shown in Table 3

Table 1: Errors of GPRIT of different h in Coil-20[30] when s =1 with different Gaussian noise

parameters	intensity of Gaussian noise						
s=1	noise free	0.001	0.002	0.003	0.004	0.005	0.006
h=−1	0.0213	0.1111	0.1364	0.1521	0.1648	0.2121	0.1854
h=−0.75	0.0202	0.0995	0.1225	0.1496	0.1401	0.1616	0.1687
h=−0.50	0.0190	0.0906	0.0998	0.1280	0.1371	0.1488	0.161
h=−0.25	0.0176	0.0815	0.1147	0.1216	0.1482	0.1487	0.1797
h=−0.00	0.0165	0.0963	0.1130	0.1353	0.1578	0.1776	0.1825
h=0.25	0.0159	0.1073	0.1527	0.1756	0.1966	0.2250	0.2480
h=0.50	0.0217	0.1611	0.2221	0.2592	0.2841	0.3138	0.3344
h=0.75	0.0241	0.2219	0.2992	0.3418	0.3816	0.4092	0.4318
AMIs	0.0008	0.7134	0.8344	0.8988	0.9415	0.9587	0.9790
MSA	0.0081	0.2611	0.3404	0.3944	0.4364	0.4673	0.4938

Secondly, affine invariant features are compared with AMIs when parameter $h=-1$, s is 0, 0.25, 0.50, 0.75, 1.00 ,1.25, 1.50, 1.75, 2.00, respectively. In this experiment, AMIs method takes 3 affine invariants and MSA method selects 29 affine invariants, and each image adds noise. Intensities of noise are 0, 0.001, 0.002, 0.003, 0.004, 0.005, and 0.006. According to Eq .(6), relative errors of GPRIT before and after adding 'salt&pepper' noise are calculated. The experimental results are as shown in Table 4. The experimental results for binary images also show that with the increase of noise, relative errors of GPRIT are smaller than that of AMIs and MSA. In other words, GPRIT is more robust.

Table 2: Errors of GPRIT of different s in Coil-20[30] when h=-1 with different Gaussian noise

parameters	intensity of Gaussian noise						
h=-1	noise free	0.001	0.002	0.003	0.004	0.005	0.006
s=0.25	0.0189	0.0833	0.1173	0.1339	0.1662	0.1685	0.1736
s=0.50	0.0203	0.0898	0.1174	0.1353	0.1478	0.1648	0.1706
s=0.75	0.0210	0.1016	0.1288	0.1391	0.1445	0.1572	0.1909
s=1.00	0.0213	0.1111	0.1364	0.1521	0.1648	0.2121	0.1854
s=1.25	0.0217	0.1290	0.1543	0.1744	0.1902	0.1753	0.2064
s=1.50	0.0225	0.1459	0.1724	0.1802	0.2011	0.2139	0.1952
s=1.75	0.0234	0.1652	0.1909	0.2044	0.2093	0.2251	0.2308
s=2.00	0.0242	0.1840	0.2109	0.2225	0.2373	0.2344	0.2422
AMIs	0.0008	0.7134	0.8344	0.8988	0.9415	0.9587	0.9790
MSA	0.0081	0.2611	0.3404	0.3944	0.4364	0.4673	0.4938

Table 3: Errors of GPRIT of different h in Fig. 2(b) when s=1 with different 'salt&pepper' noise

parameters	intensity of 'salt&pepper' noise						
s=1	noise free	0.001	0.002	0.003	0.004	0.005	0.006
h=−1	0.0426	0.0595	0.0784	0.1144	0.1322	0.1639	0.1937
h=−0.75	0.0361	0.0582	0.0823	0.1107	0.1376	0.1590	0.1836
h=−0.50	0.0295	0.0479	0.0750	0.0904	0.1148	0.1351	0.1740
h=−0.25	0.0259	0.0418	0.0643	0.0919	0.1071	0.1188	0.1419
h=−0.00	0.0242	0.0376	0.0526	0.0766	0.0868	0.105	0.1143
h=0.25	0.0222	0.0347	0.0425	0.0634	0.0761	0.0915	0.0983
h=0.50	0.0332	0.0448	0.0589	0.0703	0.0888	0.0998	0.1095
h=0.75	0.0358	0.0818	0.117	0.1539	0.1917	0.2228	0.2503
AMIs	0.0092	0.7979	1.4354	2.1057	2.5642	3.2236	3.5866
MSA	0.0274	0.2010	0.2509	0.2914	0.3835	0.4184	0.4934

Affine transforms are generated by the following transform matrix:

$$T = k\begin{pmatrix}\cos\theta & -\sin\theta\\ \sin\theta & \cos\theta\end{pmatrix}\begin{pmatrix}a & b\\ 0 & 1/a\end{pmatrix} \tag{4.2}$$

where $k\in\{0.8,1.2\}$, $\alpha\in\{1,2\}$, $\theta\in\{0^{\circ},72^{\circ},144^{\circ},216^{\circ},288^{\circ}\}$, $b\in\{-1.5,-1,-0.5,0,0.5,1,1.5\}$. Therefore, each image is transformed 140 times. In the following experiments, the classification accuracy is defined as:

$$\eta = \frac{n_r}{N_t} \times 100\%,$$

where n_r denotes the number of correctly classified images, N_t denotes a total number images applied in test.

Table 4: Errors of GPRIT of different s in Fig. 2(b) when h=-1 with different 'salt&pepper' noise

parameters	intensity of 'salt&pepper' noise						
h=-1	noise free	0.001	0.002	0.003	0.004	0.005	0.006
s=0.25	0.0272	0.0439	0.0666	0.0881	0.1124	0.1265	0.1525
s=0.50	0.0309	0.0485	0.0739	0.0975	0.1200	0.1372	0.1745
s=0.75	0.0370	0.0619	0.0775	0.1078	0.1308	0.1504	0.1997
s=1.00	0.0426	0.0566	0.0850	0.1190	0.1470	0.1685	0.2016
s=1.25	0.0447	0.0618	0.0905	0.1172	0.1491	0.1742	0.1802
s=1.50	0.0417	0.0632	0.0826	0.1068	0.1224	0.1705	0.1994
s=1.75	0.0446	0.0720	0.1050	0.1312	0.1563	0.1669	0.2087
s=2.00	0.0483	0.0793	0.1028	0.1364	0.1496	0.2106	0.2307
AMIs	0.0092	0.7979	1.4354	2.1057	2.5642	3.2236	3.5866
MSA	0.0274	0.2010	0.2509	0.2914	0.3835	0.4184	0.4934

Considering the influence of the parameter of GPRIT and the intensities of Gaussian noise on extraction of affine invariant features. In this experiment, we still select 20 gray-scale images in Coil-20[30] and 30 fish images in Fig. 2(a) as test images. Firstly, the affine invariant features are compared with AMIs and MSA when parameter $s=1$, h is -1.00, -0.75, -0.50, -0.25, 0.00, 0.25, 0.50, 0.75, respectively. The experimental results are as shown in Fig. 3(a) and Fig. 3(b). Secondly, the affine invariant features are compared with AMIs and MSA when parameter $h=-1$, s is 0, 0.25, 0.50, 0.75, 1.00 ,1.25, 1.50, 1.75, 2.00, respectively. In this experiment, AMIs method takes 3 affine invariants and MSA method selects 29 affine invariants, the mean value of Gaussian noise is 0, and the intensities of Gaussian noise are 0, 0.001, 0.002, 0.003, 0.004, 0.005, and 0.006, respectively. The experimental results are as shown in Fig. 3(c) and Fig. 3(d). With the increase of noise, accuracy of AMIs and MSA decreases obviously. Accuracy of GPRIT decreases with the increase of noise intensity. However, accuracy of GPRIT is higher than that of AMIs and MSA when intensity of noise is same. That is to say, the invariants constructed based on GPRIT have better robust performance.

Considering the influence of the parameter of GPRIT and the intensities of 'salt&pepper' noise on extraction of affine invariant features. In this experiment, we still select Fig. 2(b) and 26 English capital letters as test image. Firstly, affine invariant features are also compared with AMIs and MSA when parameter $s=1$, h is -1, -0.75, -0.50, -0.25, 0.00, 0.25, 0.50, 0.75, respectively. The experimental results are as shown in Fig. 4(a) and Fig. 4(b). Secondly, affine invariant features are compared with AMIs and MSA when parameter $h=-1$, s is 0, 0.25, 0.50, 0.75, 1.00 ,1.25, 1.50, 1.75, 2.00, respectively. In this experiment, AMIs method takes 3 affine invariants and MSA method selects 29 affine invariants, and each image adds 'salt&pepper' noise. Intensities of noise are 0, 0.001, 0.002, 0.003, 0.004, 0.005, and 0.006. The experimental results are as shown in Fig. 4(c) and Fig. 4(d).

With the increase of noise, the accuracy of AMIs and MSA decreases obviously. Accuracy of GPRIT decreases with the increase of noise intensity. However, the accuracy of GPRIT is higher than that of AMIs and MSA. That is to say, the invariants constructed based on GPRIT have better robust performance.

Experiments are carried out on binary images, and the results are consistent with gray-scale images. So it can be concluded that more robust GPRIT can be utilized for extracting image features

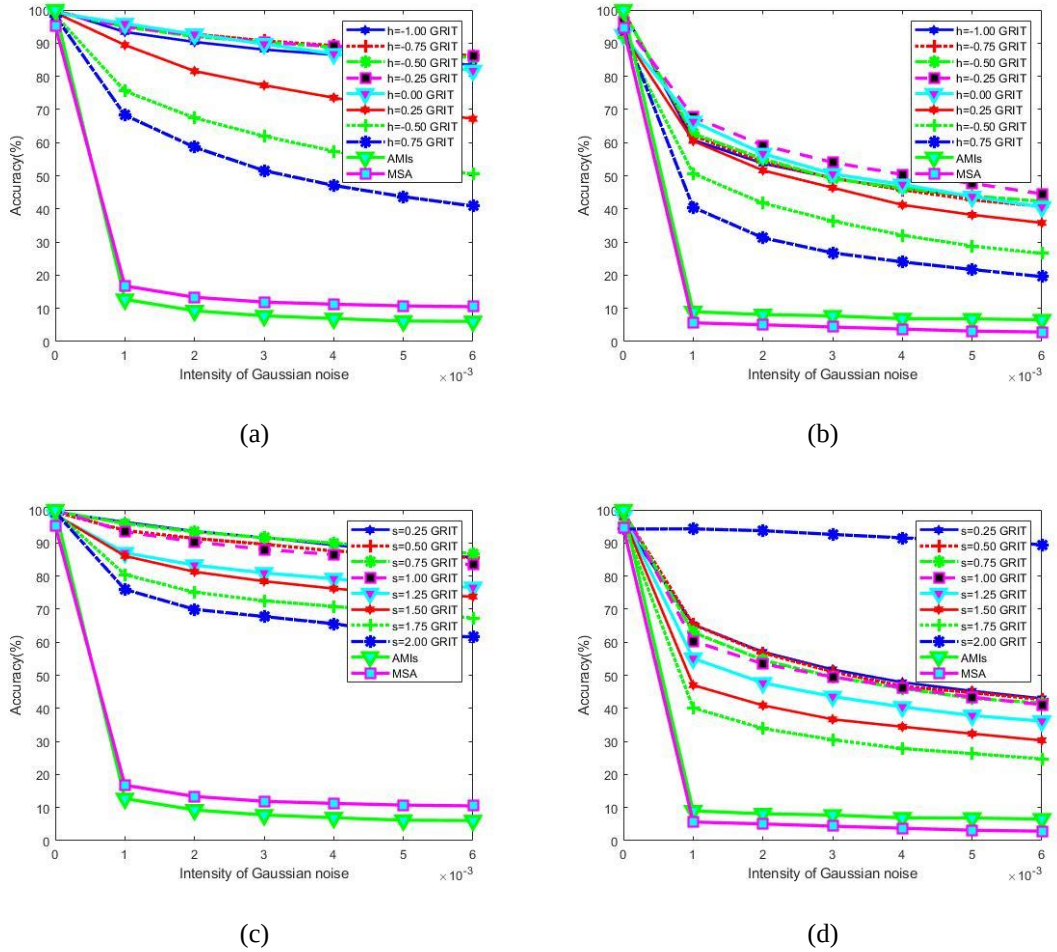

Fig. 3: (a) Accuracy of GPRIT of different h in Coil-20[30] when s=1 with different Gaussian noise. (b) Accuracy of GPRIT of different h in Fig. 2(a) when s=1 with different Gaussian noise. (c) Accuracy of GPRIT of different s in Coil-20[30] when h=-1 with different Gaussian noise. (d) Accuracy of GPRIT of different s in Fig. 2(a) when h=-1 with different Gaussian noise.

5. Conclusion

To extract affine invariant features, GPRIT is proposed in this paper. With GPRIT, any image is converted into a closed curve. The obtained closed curve is firstly parameterized to establish one-to-one points correspondence between GPRITs of the image and its transformed version. Then SWT is conducted on the parameterized GPRIT. Finally, Fourier transform is applied to derive affine invariants. The proposed GPRIT is the generation of PRIT and CPT. Experiments have also been conducted to demonstrate performance of the proposed method. Results show that the proposed method is robust to noise.

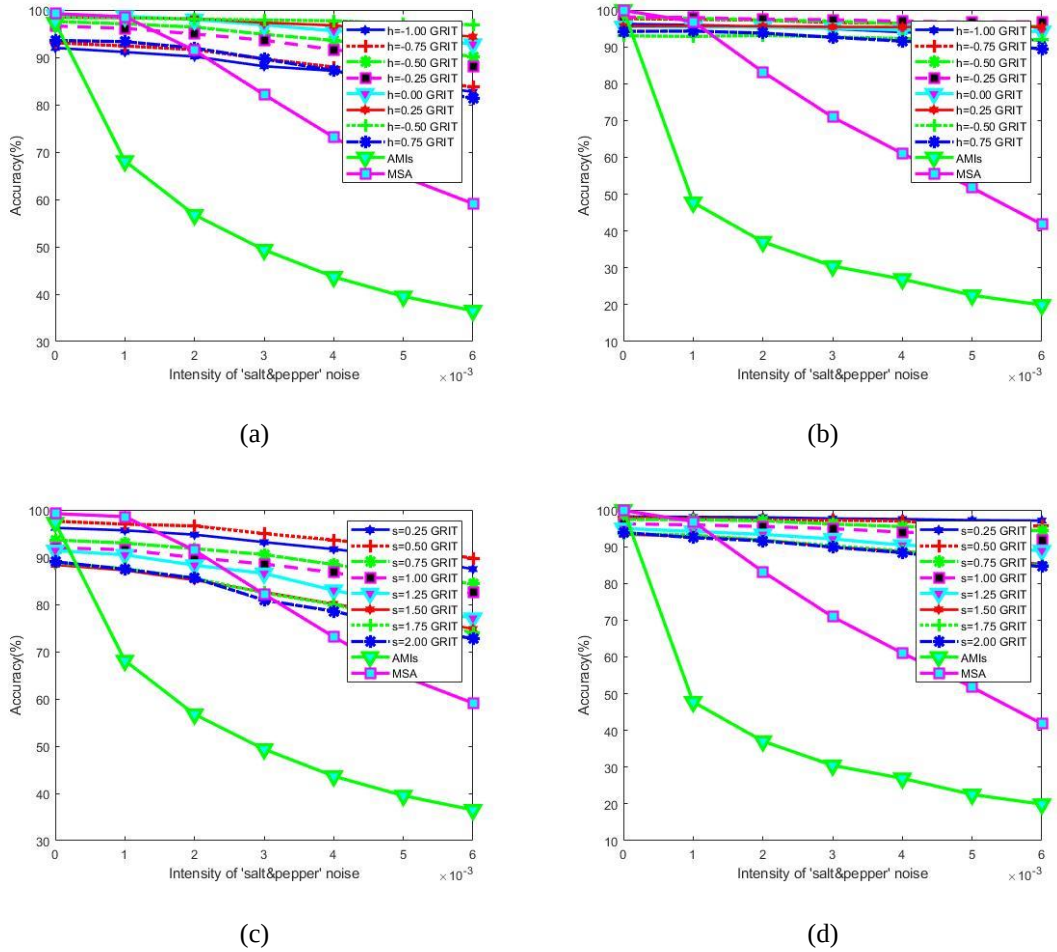

Fig. 4: (a) Accuracy of GPRIT of different h in Fig. 2(b) when s =1 with different 'salt&pepper' noise. (b) Accuracy of GPRIT of different h in Fig. 2(c) when s =1 with different 'salt&pepper' noise. (c) Accuracy of GPRIT of different s in Fig. 2(b) when h=-1 with different 'salt&pepper' noise. (d) Accuracy of GPRIT of different s in Fig. 2(c) when h=-1 with different 'salt&pepper' noise.

6. Acknowledgements

This work was supported in part by the National Science Foundation under Grant 61572015.

7. References

[1] D. Bryner, E. Klassen, H. Le, and A. Srivastava, *2D affine and projective shape analysis*, IEEE Transactions on Pattern Analysis and Machine Intelligence, 36(2014), pp. 998-1011.

[2] L. Diao, Z. Zhang, Y. Liu, and D. Nan, *Necessary condition of affine moment invariants*, Journal of Mathematical Imaging and Vision, 61(2019), pp. 602-606.

[3] T. Suk, J. Flusser, and B. Zitova, *2D and 3D image analysis by moments*, Jonh Wiley and Sons, 2016.

[4] X. Dai, H. Zhang, T. Liu, H. Shu, and L. Luo, *Legendre moment invariants to blur and affine transformation and their use in image recognition*, Pattern Analysis and Applications, 17(2014), pp. 311-326.

[5] M. Gong, Y. Hao, H. Mo, and H. Li, *Naturally combined shape-color moment invariants under affine transformations*, Computer Vision and Image Understanding, 162(2017), pp. 46-56.

[6] Y. Hao, Q. Li, H. Mo, H. Zhang, and H. Li, *AMI-Net: Convolution neural networks with affine moment invariants*, IEEE Signal Processing Letters, 25(2018), pp. 1064-1068.

[7] B. Zitova, J. Flusser, *Image registration methods: a survey*, Image and Vision Computing, 21(2003), pp. 977-1000.

[8] Y. O. Tak, P. D. Sung, K. S. Hee, K. K. Eun, L. M. Taeg, and K. T. Koo, *Pattern matching for industrial object recognition using geometry-based vector mapping descriptors*, Pattern Analysis and Applications, 21(2018), pp. 1167-1183.

[9] C. Wang, X. Wang, and Z. Xia, *Geometrically invariant image watermarking based on fast Radial Harmonic Fourier Moments*, Signal Processing: Image Communication, 45(2016), pp. 10-23.

[10] Z. H. Shao, Y. Y. Shang, R. Zeng, H. Z. Shu, G. N. Goatrieux, and J. S. Wu, *Robust watermarking scheme for color image based on quaternion-type moment invariants and visual cryptography*, Signal Processing: Image Communication, 48(2016), pp. 12-21.

[11] H. Yang, S. Qi, C. Wang, S. Yang, and X. Wang, *Image analysis by log-polar Exponent-Fourier moments*, Pattern Recognition, 101, 107177, 2020.

[12] B. Xiao, J. X. Luo, X. L. Bi, W. S. Li, and B. J. Chen, *Fractional discrete Tchebyshev moments and their applications in image encryption and watermarking*, Information Science, 516(2020), pp. 545-549.

[13] D. S. Zhang, and G. J. Lu, *Review of shape representation and description techniques*, Pattern Recognition, 37(2004), pp. 1-19.

[14] K. Arbter, W. E. Synder, H. Burkhardt, and et al, *Application of affine-invariant Fourier descriptors to recognition of 3-D objects*, IEEE Trans. Pattern Analysis and Machine Intelligence,12(1990), pp. 640–647.

[15] M. I. Khalil, and M. M. Bayoumi, *A dyadic wavelet affine invariant function for 2D shape recognition*, IEEE Trans. Pattern Analysis and Machine Intelligence, 23(2001), pp. 1152–1163.

[16] I. E. Rube, M. Ahmed, and M. Kamel, *Wavelet approximation-based affine invariant shape representation functions*, IEEE Trans. Pattern Analysis and Machine Intelligence, 28(2006), pp. 323–327.

[17] B. Xiao, J. X. Luo, X. L. Bi, W. S. Li, and B. J. Chen, *Fractional discrete Tchebyshev moments and their applications in image encryption and watermarking*, Information Science, 516(2020), pp. 545-549.

[18] K. Arbter, G. Hirzinger, W. Snyder, and H. Burkhardt, *Application of affine-invariant fourier descriptors to recognition of 3d-objects*, IEEE Transactions on Pattern Analysis and Machine Intelligence, 12(1990), pp. 640-647.

[19] Q. M. Tieng, and W. W. Boles, *Wavelet-based affine invariant representation: a tool for recognizing planar objects in 3d space*, IEEE Transactions on Pattern Analysis and Machine Intelligence, 19(1997), pp. 846-857.

[20] M. I. Khalil, and M. M. Bayoumi, *Affine invariants for object recognition using the wavelet transform*, Pattern Recognition Letters, 23(2002), pp.57-72.

[21] I. E. Rube, Ahmed, and M. Kamel, *Wavelet approximation-based affine shape representation functions*, IEEE Transactions on Pattern Analysis and Machine Intelligence, 23(2002), pp. 57-72.

[22] J. Flusser, and T. Suk, *Pattern recognition by affine moment invariants*, Pattern Recognition, 26(1993), pp.167–174.

[23] T. Suk, and J. Flusser, *Affine moment invariants generated by graph method*, Pattern Recognition, 44 (2011), pp. 2047–2056

[24] Z. Yang, and F. Cohen, *Cross-weighted moments and affine invariants for image registration and matching*, IEEE Transactions on Pattern Analysis and Machine Intelligence, 21(1999), pp. 804-814.

[25] E. Rahtu, M. Salo, and J. Heikkila, *Affine invariant pattern recognition using multiscale autoconvolution, IEEE Trans*. Pattern Analysis and Machine Intelligence, 27(2005), pp. 908–918.

[26] Y. Y. Tang, and Y. Tao, *New method for feature extraction based on fractal behavior*, Pattern Recognition, 35(2002), pp. 1071–1081.

[27] Y. D. Huang, Y. J. Yang, S. S. Li, and W. Z. Du, *Polar radius integral transform for affine invariant feature extraction*, International Journal of Wavelets Multiresolution and Information Processing, 15(2016), pp. 640-647.

[28] J. W. Yang, and R. S. Lan, *Affine invariance of central projection transformation*, Acta Electronica Sinica, 11(2012) pp. 2315–2319.

[29] R. S. Lan, J. W. Yang, Y. Jiang, and et al, *Whitening central projection descriptor for affine invariant shape description*, IET Image Processing, 7(2013), pp. 81–91.

[30] M. Q. Yang, K. Kpalma, J. Ronsin. *Affine invariance contour descriptor based on the equal area normalization* . LAENG International Journal of Applied Mathematics, 36(2007), pp. 1-6.

[31] M. Q. Yang, K. Kpalma, and J. Ronsin, *Affine invariance contour descriptor based on the equal area normalization*, LAENG International Journal of Applied Mathematics 36(2007), pp. 2.

[32] http://www1.cs.columbia.edu/CAVE/software/softlib/coil 20.php.

[33] I. E. Rube, M. Ahmed, and M. Kamel, *Wavelet approximation- based affine invariant shape rtepresentation functions*, IEEE Trans on PAMI, 28(2006) , pp. 323- 327.